

ROLUL ENTROPIEI CONFIGURAȚIONALE ÎN SISTEME OXIDICE DE TIP FLUORIT – SCURTĂ RECENZIE

THE ROLE OF CONFIGURATIONAL ENTROPY IN FLUORITE OXIDES SYSTEMS: A MINI-REVIEW

VASILE – ADRIAN SURDU* , ECATERINA ANDRONESCU

Department of Science and Engineering of Oxide Materials and Nanomaterials, Faculty of Applied Chemistry and Materials Science, Politehnica University of Bucharest

Configurational entropy has been recently used to develop innovative materials with multiple different cations or anions, belonging to different crystallographic systems. Fluorite oxides exhibit chemical stability, thermal stability and thermal insulating properties and therefore are of interest in high temperature applications. Entropy engineering via compositional considerations proved to be beneficial in increasing hardness and decreasing thermal conductivity coefficient. Several aspects need to be considered and investigated in order to understand the mechanisms involved in the functionality of such materials.

Entropia configurațională a fost recent utilizată pentru a dezvolta materiale inovatoare cu cationi sau anioni diferiți, aparținând diferitelor sisteme cristalografice. Oxizii de tip fluorit prezintă stabilitate chimică, stabilitate termică și proprietăți de izolare termică și, prin urmare, sunt de interes în aplicații la temperaturi ridicate. Ingineria entropiei prin considerații compoziționale s-a dovedit a fi benefică în creșterea durității și scăderea coeficientului de conductivitate termică. Mai multe aspecte trebuie luate în considerare și investigate pentru a înțelege mecanismele implicate în funcționalitatea acestor materiale.

Keywords: ceramics, entropy, fluorites, oxides.

1. Introduction

Configurational entropy was recently used to stabilize solid solution alloys into single-phase crystalline materials. This led to a new class of alloys called high-entropy alloys (HEAs) or multi-principal element alloys comprised of a random arrangement of more than 4 metallic components in near-equiatomic proportions (chemical disorder) [1,2].

Cantor's and Yeh's work [3,4] on alternative approach consisted in exploration of higher order diagrams where compositions containing near equal amounts of components showed that high mixing entropy, $\Delta S_{\text{mix}} = -R \sum x_i \ln x_i$, where S_{mix} is the mixing entropy, R is the gas constant and x_i is the mole fraction of component i, seem to form significantly fewer phases than that dictated by the Gibbs Phase Rule [5,6]. Considering the number of components and the atomic concentration of each component, there are three types of compositions: equimolar, non-equimolar (when the number of components is more than 4 and $5\% \leq x_i \leq 35\%$) and minor elemental additions (when $x_i \leq 5\%$). Besides this composition considerations, the scientific community has agreed on four characteristics that are expected to have an influence on the composition-structure-property relationship of high entropy alloys:

- i. The high entropy effect: a mixing entropy of $1.61R$ calculated for an equimolar 5-component solid solution is expected to enhance the potential for solid solution formation at high temperatures.

- ii. Slow kinetics: the diffusion coefficients are lower comparing to corresponding conventional alloys
- iii. Severe lattice distortion: the lattice distortions are caused by the differences in atomic size of the constituents
- iv. The synergistic effect: amplified effects can arise from the combined interactions between the components which may lead to improved or new properties.

Most of the work concerning configurational entropy refers to alloys. In what concerns ceramics, only a couple of high-entropy ceramic (HEC) structures have been successfully fabricated. Comparing with HEAs, HECs family possess structural diversity and may be divided in: rock salt, fluorite, perovskite, spinel, Half Heusler, zinc blende, CrSi₂-type and AlB₂-type[7]. Rock salt structured ceramics with (Co_{0.2}Cu_{0.2}Mg_{0.2}Ni_{0.2}Zn_{0.2})O composition were the first discovered HECs by Rost et al.[8] and consequently the most studied. Several papers show the entropy stabilization effect, investigate the crystal structure and the disorder at different length scales and explore new or improved functionalities in several derivatives of this system containing additional elements like Li, Na, Ga or K. Studies regarding the previously mentioned systems showed promising ion-conducting and dielectric properties useful for electrochemical energy storage with composition-based tailorable properties[9]. The interest in high entropy ceramics in the scientific community, evaluated by the number of publications by year (Fig. 1) shows an ascending trend starting

* Autor corespondent/Corresponding author,
E-mail: adrian.surdu@upb.ro

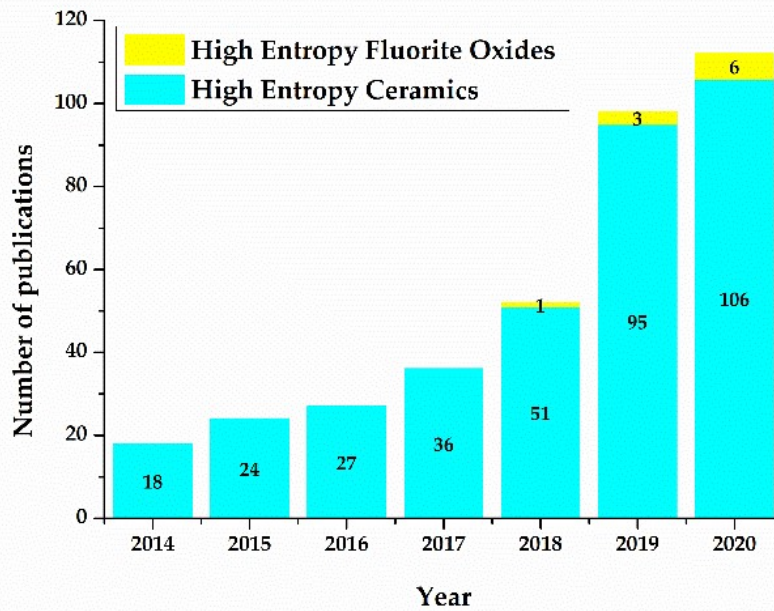


Fig. 1 - Publications about high entropy ceramics and high entropy fluorite oxides by year. Data available from Web of Science until 2020 / Publicații referitoare la ceramică cu entropie ridicată cu structură de tip fluorit. Date disponibile de pe Web of Science până în 2020

with the work of Christina Rost in 2014. Since then, researchers and engineers studied various compositions and structures possessing configurational entropy, including high entropy fluorite oxides.

Configurational entropy in fluorite oxide systems might have an important influence in obtaining improved properties highly demanded in aerospace, automotive and energy applications which require increased operating temperature and low thermal conductivity [10].

This minireview focuses on the latest findings in what concerns synthesis, processing and properties of high entropy fluorite oxides.

2. Fluorite oxide structure

In oxides with fluorite-type structure (MO_2), M^{4+} and O^{2-} ions are located at $4a$ (0, 0, 0) and $8c$ ($\frac{1}{4}$, $\frac{1}{4}$, $\frac{1}{4}$) sites, respectively, in the cubic $Fm-3m$ space group (Fig. 2).

In pure state, the actinide dioxides have cubic fluorite-type structure and are the most important characteristic oxides of the series.

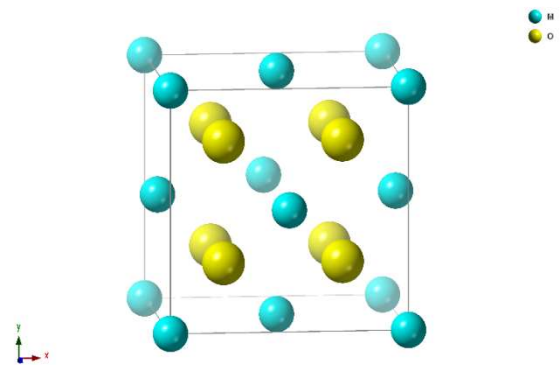


Fig. 2- Crystal structure of a fluorite-type structured MO_2 / Structură cristalină de tip fluorit MO_2

Table 1 summarizes their lattice parameters [11–15], coordination number, cation radius [16] and melting point [17–20].

Actinide dioxides are used as nuclear fuels explicitly or in mixtures called mixed oxide fuel (MOX) [19]. These are high-melting point, refractory oxides and show decreasing average melting point, lattice parameters and cation radius in series.

Table 1

Lattice parameters, cation coordination number, cation radius and average melting point of actinide dioxides
Parametrii rețelei cristaline, numărul de coordonare al cationilor, raza cationică și punctul mediu de topire ai oxizilor actinidelor

Chemical formula	Lattice parameters [Å]	Cation coordination number	Cation radius [Å]	Average melting point [K]
ThO_2	5.5975	8	1.05	3643
PaO_2	5.5050	8	1.01	-
UO_2	5.4704	8	1	3120
NpO_2	5.4340	8	0.98	3070
PuO_2	5.3977	8	0.96	3017
AmO_2	5.3888	8	0.95	-
CmO_2	5.3642	8	0.95	-
BkO_2	5.3400	8	0.93	-
CfO_2	5.3100	8	0.92	-

Relatively smaller-sized cations (Hf^{4+} and Zr^{4+}) have a largely distorted monoclinic baddeleyite-type structure at room temperature. However, at high temperatures or by using substituents or dopants, these oxides also stabilize in fluorite system [21,22]. This approach was intensively studied and applied in structural, electronic or magnetic systems. Doping strategy induces local chemical disorder, which results in stabilizing fluorite structure and generation of point defects when heterovalent ions are used for this purpose. A new strategy adopted by several research groups, consists of structure stabilization by entropy induced by designing multicomponent chemical compositions.

3. Compositionally Complex Fluorite Oxides (CCFO)

Djenadic and Sarkar [23,24] investigated multicomponent equimolar fluorite oxide systems containing three to seven of the following rare earth cations: Ce^{4+} , Gd^{3+} , La^{3+} , Nd^{3+} , $\text{Pr}^{3+/4+}$, Sm^{3+} , Y^{3+} . The results obtained by the authors from diffractometry, microscopy, and spectroscopy analyses on powders obtained from nitrate precursors by nebulized spray pyrolysis demonstrate presence of crystalline powders with fluorite structure, $Fm-3m$ space group for following compositions: CeO_2 , $(\text{Ce,Pr})\text{O}_{2-5}$, $(\text{Ce,La,Pr})\text{O}_{2-5}$, $(\text{Ce,La,Pr,Sm})\text{O}_{2-5}$, $(\text{Ce,La,Pr,Y})\text{O}_{2-5}$, $(\text{Ce,La,Pr,Sm,Y})\text{O}_{2-5}$, $(\text{Ce,La,Nd,Pr,Sm,Y})\text{O}_{2-5}$, $(\text{Ce,La,Nd,Pr,Sm,Y})\text{O}_{2-5}$. Upon calcination at 1000°C , the compositions with the highest unit cell parameters show bixbyte structure, $Ia-3$ space group. This might be the first experiment where entropy stabilization at low temperatures combined with point defects generation and mixing efficiency during bottom-up synthesis techniques led to fluorite-structure stabilization. Cyclic heat-treatment analysis of phase transformations would be beneficial to further clarify this aspect. Sajid *et al.* [25] highlighted the importance of selecting the starting component with Ce^{4+} addition to improve single-phase solid solution formation.

Entropy stabilization in the temperature range $1100-1200^\circ\text{C}$ for $(\text{Ce}_{0.20}\text{Zr}_{0.20}\text{Y}_{0.20}\text{Gd}_{0.20}\text{La}_{0.20})\text{O}_{2-5}$ obtained by hydrothermal treatment of solutions containing nitrate precursors was observed by Spiridigliozzi *et al.* [26]. Cyclic heat treatments show entropy stabilization in the case of

$(\text{Ce}_{0.20}\text{Zr}_{0.20}\text{Y}_{0.20}\text{Gd}_{0.20}\text{La}_{0.20})\text{O}_{2-5}$ prepared using ammonia as mineralizer.

Unit cell parameters for (Hf, Zr, Ce) core cubic fluorite-type structures (Table 2) reported by several authors [27–29] increases with the addition of larger ions comparing to reference Zr^{4+} . Moreover, due to stabilization in this structure, cations in a smaller oxidation state than 4+ change their coordination number to a higher value, 8, during solid solution formation, thus leading to the increase of the ionic radius of the species. The difference in charge is compensated by oxygen vacancies generation, which play an important role in the defect chemistry, and hence on the functional properties of the material.

Relative densities measurements within presented data showed values $> 95\%$ with three exceptions: $(\text{Hf}_{0.25}\text{Zr}_{0.25}\text{Ce}_{0.25}\text{Yb}_{0.125}\text{Gd}_{0.125})\text{O}_{2-5}$, $(\text{Hf}_{0.2}\text{Zr}_{0.2}\text{Ce}_{0.2}\text{Y}_{0.2}\text{Yb}_{0.2})\text{O}_{2-5}$ and $(\text{Hf}_{0.2}\text{Zr}_{0.2}\text{Ce}_{0.2}\text{Yb}_{0.2}\text{Gd}_{0.2})\text{O}_{2-5}$, after processing at 1650°C by Spark Plasma Sintering (SPS). In the case of the last two compositions, increasing the SPS temperature at 1800°C has a beneficial effect on obtaining fully dense ceramics with a relative density of 98.2%.

Zhao *et al.* [30] designed and synthesized a defective fluorite structured $(\text{Y}_{0.25}\text{Yb}_{0.25}\text{Er}_{0.25}\text{Lu}_{0.25})_2(\text{Zr}_{0.5}\text{Hf}_{0.5})_2\text{O}_7$ by solid-state reaction method from oxide precursors using ball-milling and spark plasma sintering. Annealing heat treatments at 1450°C and 1590°C with different soaking times demonstrate the sluggish grain growth due to complex composition. Experiments show a similar grain growth rate at 1450°C for high entropy $(\text{Y}_{0.25}\text{Yb}_{0.25}\text{Er}_{0.25}\text{Lu}_{0.25})_2(\text{Zr}_{0.5}\text{Hf}_{0.5})_2\text{O}_7$ and $\text{Y}_2\text{Zr}_2\text{O}_7$ reference sample. When analysing grain sizes obtained by annealing at 1590°C at various times between 0 and 18 h, there is evidence of a much lower rate of $0.151 \mu\text{m}^2/\text{h}$ in the case of $(\text{Y}_{0.25}\text{Yb}_{0.25}\text{Er}_{0.25}\text{Lu}_{0.25})_2(\text{Zr}_{0.5}\text{Hf}_{0.5})_2\text{O}_7$ in contrast with $0.328 \mu\text{m}^2/\text{h}$ observed for $\text{Y}_2\text{Zr}_2\text{O}_7$. Moreover, the high-entropy composition shows a narrow grain size distribution. The study was developed in what concerns composition to rare-earth niobates and tantalates [31]. X-ray diffraction, scanning electron microscopy and electron dispersive spectroscopy measurements showed pure phases with homogeneous distribution of the elements for $(\text{Y}_{1/3}\text{Yb}_{1/3}\text{Er}_{1/3})_3\text{TaO}_7$, $(\text{Y}_{1/3}\text{Yb}_{1/3}\text{Er}_{1/3})_3\text{NbO}_7$ and $(\text{Sm}_{1/6}\text{Eu}_{1/6}\text{Y}_{1/6}\text{Yb}_{1/6}\text{Lu}_{1/6}\text{Er}_{1/6})_3(\text{Nb}_{1/2}\text{Ta}_{1/2})\text{O}_7$ with defective fluorite structure and relative densities higher than 99%.

Table 2

Summarized sintering temperature and physical properties in single-phase YSZ and compositionally complex ceramics fluorite oxides
Condițiile tratamente termice de sinterizare și proprietățile fizice ale YSZ și ceramicilor compozițional complexe de tip fluorit [27–29]

Composition	Sintering temperature (°C)	Cubic			Tetragonal		Relative Density [%]	Nanohardness [GPa]	E [Gpa]	k [W·m ⁻¹ ·K ⁻¹]	E/k [Gpa·m·K·W ⁻¹]
		a(Å)	a(Å)	c(Å)	a(Å)	c(Å)					
8YSZ	SPS/1800	5.134	—	—	—	—	97.3 ± 0.6	17.3 ± 1.5	219.2 ± 2.6	2.19 ± 0.07	100.3 ± 3.2
(Hf _{0.314} Zr _{0.314} Ce _{0.314} Y _{0.029} Yb _{0.029})O _{2-δ}	SPS/1800	—	3.682	5.238	—	—	96.9 ± 0.6	17.1 ± 1.8	201.2 ± 2.2	1.78 ± 0.05	113.0 ± 3.6
(Hf _{0.314} Zr _{0.314} Ce _{0.314} Y _{0.029} Gd _{0.029})O _{2-δ}	SPS/1800	—	3.69	5.245	—	—	96.1 ± 0.6	18.5 ± 1.4	199.4 ± 2.0	1.74 ± 0.05	114.3 ± 3.6
(Hf _{0.314} Zr _{0.314} Ce _{0.284} Y _{0.029} Ca _{0.029})O _{2-δ}	SPS/1800	5.214	—	—	—	—	97.3 ± 0.6	18.4 ± 1.3	180.1 ± 4.8	1.65 ± 0.05	109.4 ± 4.4
(Hf _{0.284} Zr _{0.284} Ce _{0.284} Y _{0.074} Yb _{0.074})O _{2-δ}	SPS/1800	5.21	—	—	—	—	97.5 ± 0.6	17.7 ± 1.7	232.8 ± 2.2	1.74 ± 0.05	133.6 ± 4.3
(Hf _{0.284} Zr _{0.284} Ce _{0.284} Y _{0.074} Gd _{0.074})O _{2-δ}	SPS/1800	5.225	—	—	—	—	96.9 ± 0.6	18.2 ± 1.7	218.9 ± 2.3	1.70 ± 0.05	128.4 ± 4.2
(Hf _{0.284} Zr _{0.284} Ce _{0.284} Y _{0.074} Ca _{0.074})O _{2-δ}	SPS/1800	5.218	—	—	—	—	95.4 ± 0.6	19.6 ± 0.6	153.8 ± 2.3	1.54 ± 0.05	99.6 ± 3.4
(Hf _{0.25} Zr _{0.25} Ce _{0.25} Y _{0.125})O _{2-δ}	SPS/1650	5.24	—	—	—	—	98.5	13.6 ± 0.5	—	1.74 ± 0.15	—
(Hf _{0.25} Zr _{0.25} Ce _{0.25} Y _{0.125} Yb _{0.125})O _{2-δ}	SPS/1650	5.23	—	—	—	—	100	12.7 ± 0.7	—	1.55 ± 0.20	—
(Hf _{0.25} Zr _{0.25} Ce _{0.25} Y _{0.125} Ca _{0.125})O _{2-δ}	SPS/1650	5.25	—	—	—	—	98.5	13.3 ± 0.6	—	1.1 ± 0.2	—
(Hf _{0.25} Zr _{0.25} Ce _{0.25} Y _{0.125} Gd _{0.125})O _{2-δ}	SPS/1650	5.25	—	—	—	—	96.4	13.2 ± 0.5	—	1.17 ± 0.13	—
(Hf _{0.25} Zr _{0.25} Ce _{0.25} Yb _{0.125} Gd _{0.125})O _{2-δ}	SPS/1650	5.25	—	—	—	—	77.8	12.6 ± 0.5	—	1.81 ± 0.14	—
(Hf _{0.25} Zr _{0.25} Ce _{0.25} Y _{0.125} Ti _{0.125})O _{2-δ}	SPS/1650	—	—	—	—	—	—	—	—	—	—
(Hf _{0.25} Zr _{0.25} Ce _{0.25} Y _{0.125} Mg _{0.125})O _{2-δ}	SPS/1650	—	—	—	—	—	—	—	—	—	—
(Hf _{0.2} Zr _{0.2} Ce _{0.2} Y _{0.2} Ca _{0.2})O _{2-δ}	SPS/1650	—	—	—	—	—	—	—	—	—	—
(Hf _{0.25} Zr _{0.25} Ce _{0.25} Y _{0.125} La _{0.125})O _{2-δ}	SPS/1650	—	—	—	—	—	—	—	—	—	—
(Hf _{0.2} Zr _{0.2} Ce _{0.2} Y _{0.2} Yb _{0.2})O _{2-δ}	SPS/1800 SPS/1650	5.227 5.24	—	—	—	—	98.2 ± 0.6 93.7	—	232.6 ± 2.4	2.23 ± 0.07 1.29 ± 0.11	104.4 ± 3.3
(Hf _{0.2} Zr _{0.2} Ce _{0.2} Y _{0.2} Gd _{0.2})O _{2-δ}	SPS/1800 SPS/1650	5.265 5.28	—	—	—	—	98.2 ± 0.6 95.8	16.3 ± 1.2 13.1 ± 0.5	238.9 ± 2.7	2.19 ± 0.06 1.61 ± 0.13	106.3 ± 3.3
(Hf _{0.2} Zr _{0.2} Ce _{0.2} Yb _{0.2} Gd _{0.2})O _{2-δ}	SPS/1650	5.27	—	—	—	—	68.4	12.3 ± 0.7	—	1.62 ± 0.13	—
(Hf _{0.2} Zr _{0.2} Ce _{0.2} Sn _{0.2} Ti _{0.2})O ₂	CS/1500	5.3518	—	—	—	—	—	—	—	1.28	—

4. Design and preparation of compositionally complex fluorite oxides

Crystals are solid materials which constituents are arranged in a highly ordered, repeating structures. This representation allows engineers and researchers to focus on a microscopic subset of unique species and positions to depict materials properties, including mechanical, electronic or magnetic features [32,33].

Predicting formation of high-entropy ceramics is challenging, owing to the complexity of the composition and the lack of the data. The disordered configuration is difficult for most computational approaches. Kaufmann *et al.* [32] developed a model on a machine-learning architecture that uses decision trees that individually make predictions on each input and the overall prediction determined by a majority voting process. The predictor used in this model can evaluate the entropy forming ability in under a millisecond and the results are in good agreement with previously reported data. To date, the model was only used to describe high entropy metal carbides.

CCFO powders are usually obtained by ball-milling followed by heat treatment [28]. This process

is simple and scalable but requires large amount of energy both for milling and for heat treatment, due to high melting points of precursors. Another approach is represented by bottom-up techniques such as nebulized spray pyrolysis, co-precipitation or hydrothermal which were reported by a few publications [23–26]. The second approach uses milder conditions for synthesis, which offer the advantage of reduced energy consumption. However, the disadvantage arises from high costs for salt precursors.

Shaping and sintering CCFO ceramics reported so far in the literature are spark plasma sintering [28] and conventional sintering [27]. Conventional sintering usually involves long dwell times at high temperature which might affect the final composition because of preferential volatilization of one of the components. Moreover, the pellets obtained after the thermal treatment are often porous possibly requiring further pulverization or sintering treatment. Another weakness of this processing method is that high-temperature phase transformation may be competitive with sintering, thus contributing to the formation of internal

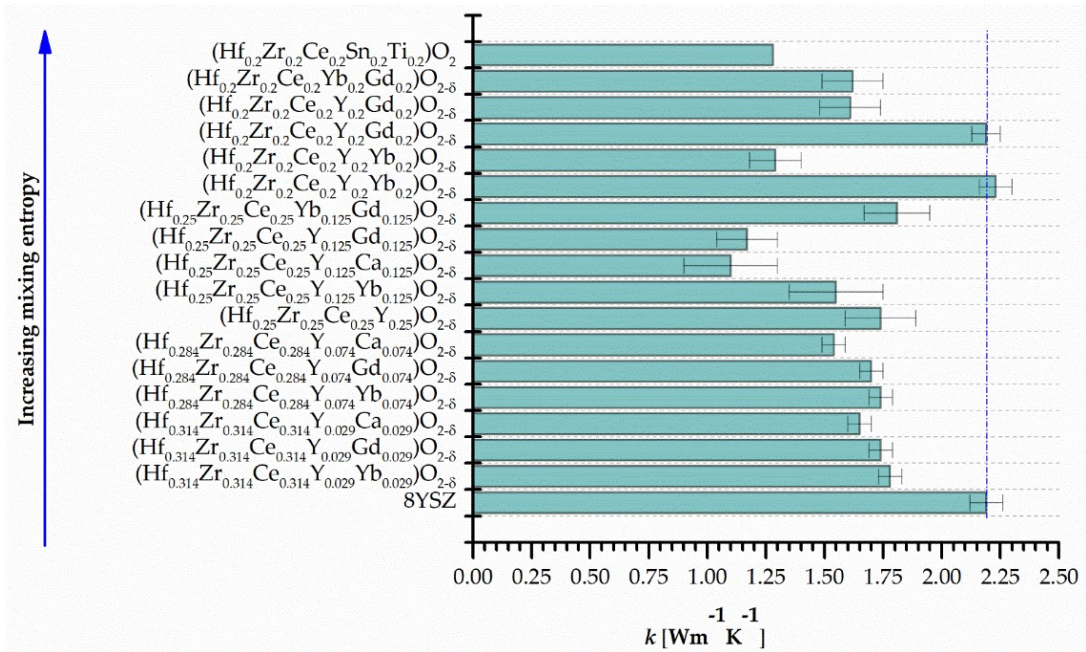


Fig. 3- Thermal conductivity of (Hf,Zr,Ce) core ceramic compositions with different additions / Conductivitatea termică a compozițiilor ceramice cu conținut de (Hf,Zr,Ce) și adaosuri diferite

stresses and physical defects [34]. These disadvantages might be overcome by using alternative methods such as SPS, flash sintering or cold sintering, which involve lower sintering temperatures, shorter dwell times or activation of consolidation process by pressure.

5. Properties of compositionally complex fluorite oxides

5.1. Thermal conductivity

Most experimental studies regarding medium and high entropy fluorite oxides have reported lowered thermal conductivity by configurational entropy but the phenomenon was not clarified yet. The available data for (Hf, Zr, Ce) core ceramic compositions with additions of MgO, CaO, SnO₂, TiO₂ or RE₂O₃ (RE = rare earth cation) obtained by SPS [27–29] are plotted in Fig. comparing to industry standard 8YSZ (8% yttria stabilized zirconia) for thermal barrier coatings.

The values depicted in Fig. 3 show a reduction of thermal conductivity from 2.02 ± 0.17 Wm⁻¹K⁻¹ for 8YSZ to 1.28 Wm⁻¹K⁻¹ for (Hf_{0.2}Zr_{0.2}Ce_{0.2}Sn_{0.2}Ti_{0.2})O₂. The difference is even larger in the case of (Hf_{0.25}Zr_{0.25}Ce_{0.25}Y_{0.125}Ca_{0.125})O_{2-δ}, which shows a thermal conductivity 1.1 ± 0.2 Wm⁻¹K⁻¹. However, the causes of this behavior lies in both intrinsic and extrinsic effects. On the one hand, increased phonon scattering due to multiple cations on the same site in the fluorite structure which cause mass and bond disorder as well as Frenkel defects can reduce measured values for thermal conductivity. On the other hand, microstructure (grain size, porosity) may also have a significant contribution [28,35–37].

5.2. Electrical conductivity

Electrical conductivity of single phase (Hf_{0.2}Zr_{0.2}Ce_{0.2}Sn_{0.2}Ti_{0.2})O₂ [27] was measured in the temperature range of 600-1100°C. The activation energy (E_a) determined by the authors from Arrhenius plot of 1.43 eV shows a semiconductor behaviour. In the case of (Hf, Zr, Ce) core CCFOs prepared by Gild *et al.* [28] the activation energies (Table 3) range between 1.14 and 1.29 eV. Besides, it was found that electrical conductivities of CCFOs are one order of magnitude lower than of 8YSZ. This aspect might be explained by higher amount of oxygen vacancies in heterovalent structures compared to (Hf_{0.2}Zr_{0.2}Ce_{0.2}Sn_{0.2}Ti_{0.2})O₂.

Table 3

Electrical conductivity of CCCs Conductivitatea electrică a CCC-urilor		
Composition	E _a [eV]	Reference
(Ce,Gd,Nd,Pr,Sm,Mo _{0.5})O _{2-δ}	0.64	[38]
(Ce,Gd,La,Nd,Pr,Mo _{0.5})O _{2-δ}	0.69	[38]
(Ce,Gd,Nd,Pr,Sm,Mo _{0.3})O _{2-δ}	0.69	[38]
(Ce,Gd,La,Nd,Pr,Mo _{0.3})O _{2-δ}	0.76	[38]
(Hf _{0.2} Zr _{0.2} Ce _{0.2} Y _{0.2} Gd _{0.2})O _{2-δ}	1.14	[28]
(Hf _{0.2} Zr _{0.2} Ce _{0.2} Y _{0.2} Yb _{0.2})O _{2-δ}	1.23	[28]
(Hf _{0.2} Zr _{0.2} Ce _{0.2} Sn _{0.2} Ti _{0.2})O ₂	1.43	[27]
(Hf _{0.25} Zr _{0.25} Ce _{0.25} Y _{0.125} Ca _{0.125})O _{2-δ}	1.23	[28]
(Hf _{0.25} Zr _{0.25} Ce _{0.25} Y _{0.125} Yb _{0.125})O _{2-δ}	1.27	[28]
(Hf _{0.25} Zr _{0.25} Ce _{0.25} Y _{0.25})O _{2-δ}	1.29	[28]

Dabrowa *et al.* [38] observed lower activation energies for single-phase (Ce,Gd,Nd,Pr,Sm,Mo_{0.5})O_{2-δ} and (Ce,Gd,La,Nd,Pr,Mo_{0.5})O_{2-δ} compared to mixed conductor Ce_{0.8}Pr_{0.2}O_{2-δ} and pure ionic conductor Ce_{0.8}Gd_{0.2}O_{2-δ} [39]. The nature of conductivity remains still unclear due to extrinsic and intrinsic

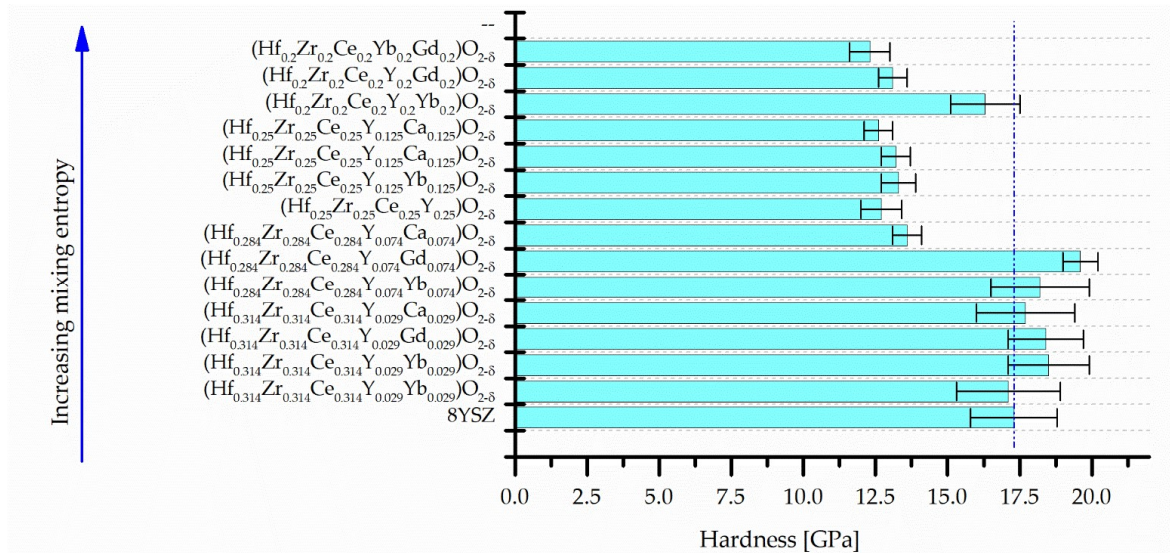


Fig. 4 - Hardness of (Hf, Zr, Ce) core ceramic compositions with different additions / *Duritatea compozițiilor ceramice cu conținut de (Hf,Zr,Ce) și adaosuri diferite.*

contributions, although the results show similarities to those reported for $\text{Ce}_{0.8}\text{Pr}_{0.2}\text{O}_{2-\delta}$ mixed ionic conductor.

5.3. Hardness

The effect of mixing entropy on hardness of ceramics is illustrated in Fig. 4.

One can see that medium entropy compositions ($\text{Hf}_{0.314}\text{Zr}_{0.314}\text{Ce}_{0.314}\text{Y}_{0.029}\text{Gd}_{0.029}\text{O}_{2-\delta}$, ($\text{Hf}_{0.314}\text{Zr}_{0.314}\text{Ce}_{0.314}\text{Y}_{0.029}\text{Ca}_{0.029}\text{O}_{2-\delta}$, ($\text{Hf}_{0.284}\text{Zr}_{0.284}\text{Ce}_{0.284}\text{Y}_{0.074}\text{Yb}_{0.074}\text{O}_{2-\delta}$) and ($\text{Hf}_{0.284}\text{Zr}_{0.284}\text{Ce}_{0.284}\text{Y}_{0.074}\text{Gd}_{0.074}\text{O}_{2-\delta}$) show higher nanohardness than reference 8YSZ. While increasing further the mixing entropy, the values of nanohardness reduce.

5.4. Thermal expansion

Thermal expansion was determined by Wright *et al.* [40] for compositions with different entropy mixing (Table 4) ($\text{Hf}_{0.314}\text{Zr}_{0.314}\text{Ce}_{0.314}\text{Y}_{0.029}\text{Yb}_{0.029}\text{O}_{2-\delta}$) and ($\text{Hf}_{0.284}\text{Zr}_{0.284}\text{Ce}_{0.284}\text{Y}_{0.074}\text{Yb}_{0.074}\text{O}_{2-\delta}$) show similar thermal expansion to 8YSZ over the studied temperature range. Higher coefficient of thermal expansion ($\approx 7\%$) observed for ($\text{Hf}_{0.2}\text{Zr}_{0.2}\text{Ce}_{0.2}\text{Y}_{0.2}\text{Yb}_{0.2}\text{O}_{2-\delta}$) may be attributed to ordering/clustering of oxygen vacancies, which was also observed for doped zirconia when oxygen vacancies exceed 5% [41–43].

6. Conclusions and future prospects

Configurational entropy leads to unexpected properties for ceramics such as high hardness, low thermal conductivity or catalyst support. The unexplored compositional space is vast, so that design methods and models of such materials would decrease the number of experiments performed on intuition of researchers.

Table 4
Coefficient of thermal expansion and oxygen vacancies in CCFOs
Coefficient de dilatare termică și vacanțe de oxigen în CCC-uri [41–43]

Composition	Coefficient of thermal expansion [K ⁻¹]	Oxygen vacancies [%]
8YSZ	$11.4 \pm 0.5 \cdot 10^{-6}$	
($\text{Hf}_{0.314}\text{Zr}_{0.314}\text{Ce}_{0.314}\text{Y}_{0.029}\text{Yb}_{0.029}\text{O}_{2-\delta}$)	$11.4 \pm 0.5 \cdot 10^{-6}$	1.5%
($\text{Hf}_{0.284}\text{Zr}_{0.284}\text{Ce}_{0.284}\text{Y}_{0.074}\text{Yb}_{0.074}\text{O}_{2-\delta}$)	$11.6 \pm 0.4 \cdot 10^{-6}$	3.7%
($\text{Hf}_{0.2}\text{Zr}_{0.2}\text{Ce}_{0.2}\text{Y}_{0.2}\text{Yb}_{0.2}\text{O}_{2-\delta}$)	$12.2 \pm 0.5 \cdot 10^{-6}$	10%

Stabilizing fluorite structure by entropy engineering is difficult to track due to high temperatures where this phenomenon occurs, for which in-situ characterization techniques are not available. The weaknesses addressed by recent papers in what concerns processing may be overcome by alternative techniques, such as processing powders in liquid phase or pressure assisted sintering. In what concerns properties, the role of entropy stabilization on thermal, mechanical, or electrical behaviour can only be assessed by taking into account in addition the nature of cations, coordination state and charge, as well as structure and microstructure. Multi-length scale characterization of the structure is a must in order to determine the mixing of elements parameter, and whether cluster formation is highlighted at a certain scale. Moreover, dimensionality of the entropy-stabilized fluorite structure may also influence phase transitions to non-centrosymmetric structures, which may lead to a change in the electrical behaviour of such solid solutions. Tailoring defect structures is another useful tool which allows control of the properties. Oxygen vacancies are the most encountered type of defects in this category of materials and clustering/ordering might play an important role for thermal and electrical behaviour.

Acknowledgements

Vasile-Adrian Surdu acknowledges the support of this work by the project ANTREPRENORDOC, in the framework of Human Resources Development Operational Programme 2014-2020, financed from the European Social Fund under the contract number 36355/23.05.2019 HRD OP /380/6/13-SMIS Code: 123847.

REFERENCES

- [1] Z. Lei, X. Liu, H. Wang, Y. Wu, S. Jiang, Z. Lu, Development of Advanced Materials via Entropy Engineering. *Scr. Mater.* 2019, **165**, 164–169, doi:10.1016/j.scriptamat.2019.02.015.
- [2] E. Castle, T. Csanádi, S. Grasso, J. Dusza, M. Reece, Processing and Properties of High-Entropy Ultra-High Temperature Carbides. *Sci. Rep.* 2018, **8**, 1–12, doi:10.1038/s41598-018-26827-1.
- [3] B. Cantor, I.T.H. Chang, P. Knight, A.J.B. Vincent, Microstructural Development in Equiatomic Multicomponent Alloys. *Mater. Sci. Eng. A* 2004, **375–377**, 213–218, doi:10.1016/j.msea.2003.10.257.
- [4] J.W. Yeh, S.K. Chen, S.J. Lin, J.Y. Gan, T.S. Chin, T.T. Shun, C.H. Tsau, S.Y. Chang, Nanostructured High-Entropy Alloys with Multiple Principal Elements: Novel Alloy Design Concepts and Outcomes. *Adv. Eng. Mater.* 2004, **6**, 299-303+274, doi:10.1002/adem.200300567.
- [5] J.W. Gibbs, On the Equilibrium of Heterogeneous Substances. *Trans. Connect. Acad. Arts Sci.* 1876, **3**, 108-248/343-524.
- [6] A. Findlay, *The Phase Rule and Its Applications*; Dover Publications, 1911; Vol. **30**.
- [7] R.Z. Zhang, M.J. Reece, Review of High Entropy Ceramics: Design, Synthesis, Structure and Properties. *J. Mater. Chem. A* 2019, **7**, 22148–22162, doi:10.1039/c9ta05698j.
- [8] C.M. Rost, E. Sachet, T. Borman, A. Moballeggh, E.C. Dickey, D. Hou, J.L. Jones, S. Curtarolo, J.P. Maria, Entropy-Stabilized Oxides. *Nat. Commun.* 2015, **6**, doi:10.1038/ncomms9485.
- [9] A. Sarkar, Q. Wang, A. Schiele, M.R. Chellali, S.S. Bhattacharya, D. Wang, T. Brezesinski, H. Hahn, L. Velasco, B. Breitung, High-Entropy Oxides: Fundamental Aspects and Electrochemical Properties. *Adv. Mater.* 2019, **31**, doi:10.1002/adma.201806236.
- [10] A. Sedegov, S. Vorotilo, V. Tsybulin, K. Kuskov, D. Moscovskikh, Synthesis and Study of High-Entropy Ceramics Based on the Carbides of Refractory Metals. *IOP Conf. Ser. Mater. Sci. Eng.* 2019, **558**, doi:10.1088/1757-899X/558/1/012043.
- [11] A.G. Seleznev, V.M. Radchenko, V.D. Shushakov, M.A. Ryabinin, R.R. Droznik, L.S. Lebedeva, V.Y. Vasil'ev, Preparation and Crystal Structure of Metallic 248Cm, 249Bk and 249Cf. *Radiokhimiya* 1989, **36**, 20–25.
- [12] P.A. Sellers, S. Fried, R.E. Elson, W.H. Zachariasen, The Preparation of Some Proactinium Compounds and the Metal. *J. Am. Chem. Soc.* 1954, **76**, 5935–5938, doi:10.1021/ja01652a011.
- [13] L. Martel, N. Magnani, J.F. Vigier, J. Boshoven, C. Selfslag, I. Farnan, J.C. Griveau, J. Somers, T. Fanghanel, High-Resolution Solid-State Oxygen-17 NMR of Actinide-Bearing Compounds: An Insight into the 5f Chemistry. *Inorg. Chem.* 2014, **53**, 6928–6933, doi:10.1021/ic5007555.
- [14] L.R. Morss, J.W. Richardson, C.W. Williams, G.H. Lander, A.C. Lawson, N.M. Edelstein, G. V. Shalimoff, Powder Neutron Diffraction and Magnetic Susceptibility of 248CmO₂. *J. Less-Common Met.* 1989, **156**, 273–289, doi:10.1016/0022-5088(89)90425-6.
- [15] R.D. Baybarz, R.G. Haire, J.A. Fahey, On the Californium Oxide System. *J. Inorg. Nucl. Chem.* 1972, **34**, 557–565, doi:https://doi.org/10.1016/0022-1902(72)80435-4.
- [16] R. Shannon, Revised Effective Ionic Radii and Systematic Studies of Interatomic Distances in Halides and Chalcogenides. *Acta Crystallogr. Sect. A* 1976, **32**, 751–767.
- [17] M. Uno, M. Katsura, M. Miyake, Preparation of Th₃N₄ and Its Oxidation Behaviour. *J. Less Common Met.* 1987, **135**, 25–38, doi:https://doi.org/10.1016/0022-5088(87)90335-3.
- [18] M.T. Hutchings, High-Temperature Studies of UO₂ and ThO₂ Using Neutron Scattering Techniques. *J. Chem. Soc. Faraday Trans. 2 Mol. Chem. Phys.* 1987, **83**, 1083–1103, doi:10.1039/F29878301083.
- [19] R. Böhler, M.J. Welland, F. De Bruycker, K. Boboridis, A. Janssen, R. Eloiirdi, R.J.M. Konings, D. Manara, Revisiting the Melting Temperature of NpO₂ and the Challenges Associated with High Temperature Actinide Compound Measurements. *J. Appl. Phys.* 2012, **111**, 1–8, doi:10.1063/1.4721655.
- [20] F. De Bruycker, K. Boboridis, P. Pöml, R. Eloiirdi, R.J.M. Konings, D. Manara, The Melting Behaviour of Plutonium Dioxide: A Laser-Heating Study. *J. Nucl. Mater.* 2011, **416**, 166–172, doi:https://doi.org/10.1016/j.jnucmat.2010.11.030.
- [21] C.G. Guizard, A.C. Julbe, Nanophase Ceramic Ion Transport Membranes for Oxygen Separation and Gas Stream Enrichment; Elsevier Masson SAS, 2000; Vol. 6;.
- [22] A. Nakamura, J. Mizusaki, *New Research Trends of Fluorite-Based Oxide Materials*; Nova Science Publishing: New York, 2015; ISBN 9788578110796.
- [23] A. Sarkar, C. Loho, L. Velasco, T. Thomas, S.S. Bhattacharya, H. Hahn, R. Djenadic, Multicomponent Equiatomic Rare Earth Oxides with a Narrow Band Gap and Associated Praseodymium Multivalency. *Dalt. Trans.* 2017, **46**, 12167–12176, doi:10.1039/c7dt02077e.
- [24] R. Djenadic, A. Sarkar, O. Clemens, C. Loho, M. Botros, V.S.K. Chakravadhanula, C. Kübel, S.S. Bhattacharya, A.S. Gandhi, H. Hahn, Multicomponent Equiatomic Rare Earth Oxides. *Mater. Res. Lett.* 2017, **5**, 102–109, doi:10.1080/21663831.2016.1220433.
- [25] S.A. Alvi, H. Zhang, F. Akhtar, High-Entropy Ceramics. In *Engineering Steels and High Entropy-Alloys*; 2019; pp. 1–22.
- [26] L. Spiridigliozi, C. Ferone, R. Cioffi, G. Accardo, D. Frattini, G. Dell'Agli, Entropy-Stabilized Oxides Owning Fluorite Structure Obtained by Hydrothermal Treatment. *Materials (Basel)*. 2020, **13**, 1–12, doi:10.3390/ma13030558.
- [27] K. Chen, X. Pei, L. Tang, H. Cheng, Z. Li, C. Li, X. Zhang, L. An, A Five-Component Entropy-Stabilized Fluorite Oxide. *J. Eur. Ceram. Soc.* 2018, **38**, 4161–4164, doi:10.1016/j.jeurceramsoc.2018.04.063.
- [28] J. Gild, M. Samiee, L. Braun, T. Harrington, H. Vega, High-Entropy Fluorite Oxides. *J. Eur. Ceram. Soc.* 2018, **38**, 3578–3584, doi:10.14311/AP.2013.53.0854.
- [29] A.J. Wright, Q. Wang, C. Huang, A. Nieto, R. Chen, J. Luo, Journal of the European Ceramic Society From High-Entropy Ceramics to Compositionally-Complex Ceramics: A Case Study of FI Uorite Oxides. *J. Eur. Ceram. Soc.* 2020, **40**, 0–1, doi:10.1016/j.jeurceramsoc.2020.01.015.
- [30] Z. Zhao, H. Chen, H. Xiang, F.-Z. Dai, W. Xu, K. Sun, Z. Peng, Y. Zhou, (Y_{0.25}Yb_{0.25}Er_{0.25}Lu_{0.25})₂(Zr_{0.5}Hf_{0.5})₂O₇: A Defective Fluorite Structured High Entropy Ceramic with Low Thermal Conductivity and Close Thermal Expansion Coefficient to Al₂O₃. *J. Mater. Sci. Technol.* 2020, **39**, 167–172, doi:10.1016/j.jmst.2019.08.018.
- [31] Z. Zhao, H. Chen, H. Xiang, F.Z. Dai, X. Wang, W. Xu, K. Sun, Z. Peng, Y. Zhou, High Entropy Defective Fluorite Structured Rare-Earth Niobates and Tantalates for Thermal Barrier Applications. *J. Adv. Ceram.* 2020, **9**, 303–311, doi:10.1007/s40145-020-0368-7.

- [32] K. Kaufmann, D. Maryanovsky, W.M. Mellor, C. Zhu, A.S. Rosengarten, T.J. Harrington, C. Oses, C. Toher, S. Curtarolo, K.S. Vecchio, Discovery of High-Entropy Ceramics via Machine Learning. *npj Comput. Mater.* 2020, **6**, 1–9, doi:10.1038/s41524-020-0317-6.
- [33] M. Howard, Introduction to Crystallography and Mineral Crystal Systems; Bob's Rock Shop, 1997;
- [34] M. Biesuz, S. Fu, J. Dong, A. Jiang, D. Ke, Q. Xu, D. Zhu, M. Bortolotti, M.J. Reece, C. Hu, et al., High Entropy Sr((Zr_{0.94}Y_{0.06})_{0.2}Sn_{0.2}Ti_{0.2}Hf_{0.2}Mn_{0.2})O_{3-x} Perovskite Synthesis by Reactive Spark Plasma Sintering. *J. Asian Ceram. Soc.* 2019, **7**, 127–132, doi:10.1080/21870764.2019.1595931.
- [35] A. Giri, J.L. Braun, P.E. Hopkins, Reduced Dependence of Thermal Conductivity on Temperature and Pressure of Multi-Atom Component Crystalline Solid Solutions. *J. Appl. Phys.* 2018, **123**, doi:10.1063/1.5010337.
- [36] A. Giri, J.L. Braun, C.M. Rost, P.E. Hopkins, On the Minimum Limit to Thermal Conductivity of Multi-Atom Component Crystalline Solid Solutions Based on Impurity Mass Scattering. *Scr. Mater.* 2017, **138**, 134–138, doi:10.1016/j.scriptamat.2017.05.045.
- [37] A. Sarkar, B. Breitung, H. Hahn, High Entropy Oxides: The Role of Entropy, Enthalpy and Synergy. *Scr. Mater.* 2020, **187**, 43–48, doi:10.1016/j.scriptamat.2020.05.019.
- [38] J. Dąbrowa, M. Szymczak, M. Zajusz, A. Mięka, M. Moździerz, K. Berent, M. Wyrwał-Sarna, A. Bernasik, M. Stygar, K. Świerczek, Stabilizing Fluorite Structure in Ceria-Based High-Entropy Oxides: Influence of Mo Addition on Crystal Structure and Transport Properties. *J. Eur. Ceram. Soc.* 2020, **40**, 5870–5881, doi:10.1016/j.jeurceramsoc.2020.07.014.
- [39] Y. Takasu, T. Sugino, Y. Matsuda, Electrical Conductivity of Praseodymia Doped Ceria. *J. Appl. Electrochem.* 1984, **14**, 79–81, doi:10.1007/BF00611261.
- [40] A.J. Wright, C. Huang, M.J. Walock, A. Ghoshal, M. Murugan, J. Luo, Sand Corrosion, Thermal Expansion, and Ablation of Medium- and High-Entropy Compositionally Complex Fluorite Oxides. *J. Am. Ceram. Soc.* 2020, 0–2, doi:10.1111/jace.17448.
- [41] J.P. Goff, W. Hayes, S. Hull, M.T. Hutchings, K.N. Clausen, Defect Structure of Yttria-Stabilized Zirconia and Its Influence on the Ionic Conductivity at Elevated Temperatures. *Phys. Rev. B* 1999, **59**, 14202–14219, doi:10.1103/PhysRevB.59.14202.
- [42] A. Bogicevic, C. Wolverton, G.M. Crosbie, E.B. Stechel, Defect Ordering in Aliovalently Doped Cubic Zirconia from First Principles. *Phys. Rev. B* 2001, **64**, 14106, doi:10.1103/PhysRevB.64.014106.
- [43] E.D. Wachsman, Effect of Oxygen Sublattice Order on Conductivity in Highly Defective Fluorite Oxides. *J. Eur. Ceram. Soc.* 2004, **24**, 1281–1285, doi:https://doi.org/10.1016/S0955-2219(03)00509-0
